Available online at www.sciencedirect.com
ScienceDirect
Journal of the European Ceramic Society 31 (2011) 2415–2423
www.elsevier.com/locate/jeurceramsoc

Toughening of laminated ZrB_2–SiC ceramics with residual surface compression

Xinghong Zhang, Peng Zhou, Ping Hu *, Wenbo Han

National Key Laboratory of Science and Technology on Advanced Composites in Special Environment, Harbin Institute of Technology, Harbin 150001, PR China

Received 26 January 2011; received in revised form 22 April 2011; accepted 17 May 2011
Available online 14 June 2011

Abstract

Laminated ZrB_2–SiC ceramics with residual surface compression were prepared by stacking layers with different SiC contents. The maximum apparent fracture toughness of these laminated ZrB_2–SiC ceramics was 10.4 $MPam^{1/2}$, which was much higher than that of monolithic ZrB_2–SiC ceramics. The theoretical predictions showed that the apparent fracture toughness was strongly dependent on the position of the notch tip, which was confirmed by the SENB tests. Moreover, laminated ceramics showed a higher fracture load when the notch tip located in the compressive layer, whereas showed a lower fracture load as the notch tip within the tensile layer. The toughening effect of residual compressive stresses was verified by the appearance of crack deflection and pop-in event. The influence of geometrical parameters on the apparent fracture toughness and residual stresses was analyzed. The results of theoretical calculation indicated that the highest residual compressive stress did not correspond to the highest apparent fracture toughness.

Keywords: Laminated structure; D. Borides; C. Toughness and toughening; C. Fracture

1. Introduction

Zirconium diboride (ZrB_2), as one of the most promising ultra-high temperature ceramic (UHTC) materials, has attracted considerable attention because of its excellent combination of physicochemical properties, such as extremely high melting point and hardness,[1,2] high thermal and electrical conductivity and excellent chemical and physical stability at high temperatures.[3] These properties make it an attractive candidate for a variety of ultra-high temperature applications, including atmospheric re-entry, hypersonic flight, and high-temperature electrodes, nozzles and armor.[2,4,5] However, despite a lot of excellent properties for different applications, the low fracture toughness directly related to the limited mechanical reliability has long prevented ZrB_2 ceramic from being used in wide structural applications.[6,7] Many attempts have been made in the past in order to improve the fracture toughness of monolithic ZrB_2 and great progress has been achieved in recent years. Generally, higher fracture toughness has been obtained through conventional approaches, including incorporation of fibers,[8] whiskers,[4,9,10] particles reinforcements,[11–13] and phase-transformation reinforcing.[6,14] Unfortunately, the unsatisfactory fracture toughness of the ZrB_2-based ceramics toughened by above-mentioned approaches is still the obstacle to a wider range of use, especially for applications in severe environments.[15] Recently, new strategies to increase toughness and improve ceramic performance have been developed that are significantly different from the conventional approach. The design of ceramic laminate to enhance the fracture toughness of ceramics is considered one of the effective strategies.[16–20] In the case of layered ceramics, there are two main methods used to enhance toughness over conventional ceramics, namely introducing low-energy paths for crack propagation[21–23] or making the presence of residual stresses.[18,24–26] For the first case, the objective has been achieved using either porous or weak interlayer to promote delamination and crack deflection. In this way the strength is usually not increased, but the deformation and the energy absorbed before failure are amplified many times.[27,28] With regard to the other case, the residual stresses in the laminated ceramics arising from a mismatch in the coefficient of thermal expansion between the different layers will remarkably enhance the fracture toughness.[29] These residual stresses can be controlled to

* Corresponding author. Tel.: +86 451 86402382; fax: +86 451 86402382.
E-mail addresses: huping@hit.edu.cn, zhoupeng85723@163.com (P. Hu).

0955-2219/$ – see front matter © 2011 Elsevier Ltd. All rights reserved.
doi:10.1016/j.jeurceramsoc.2011.05.024

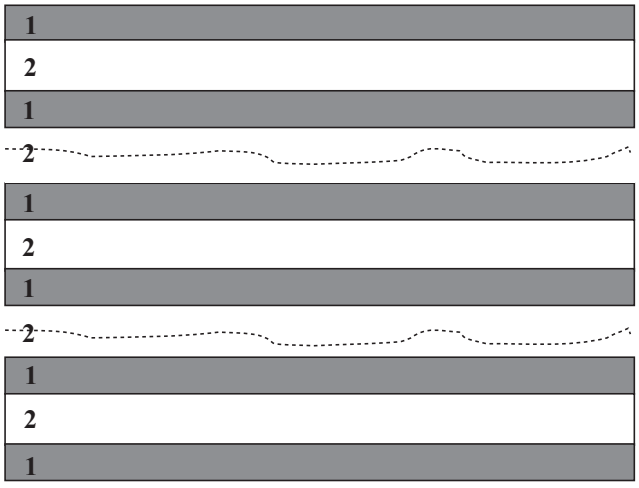

Fig. 1. Schematic illustration of the designed two-component laminated ZrB_2–SiC composite with symmetric macrostructure: the two components were signed by symbols 1 and 2, respectively.

improve their mechanical properties.[28] On ceramics and glasses, for instance, the compressive stresses on the surface have proved to be useful for increasing their fracture strength. In addition, laminated ceramics designed with compressive stresses in the bulk may present a threshold strength below which catastrophic failure does not occur.[26,28,30]

However, up to date the research on the laminated ZrB_2-based ceramics with strong interfaces has been rarely reported. In the present work, symmetrical *N*-layer laminated ZrB_2–SiC ceramics with compressive stresses at the surface were designed and prepared (*N* being an odd number to satisfy the condition of symmetry). The effect of architectural parameters on the residual stress profile and fracture toughness was investigated in detail. Furthermore, the influence of residual stresses on the mechanical performance and fracture behavior of the laminated ZrB_2–SiC ceramics was also studied.

2. Theoretical background and design

In this work two-component laminated ZrB_2–SiC ceramics composites with symmetric macrostructure are considered as shown in Fig. 1. As can be seen from Fig. 1, the layers of the first component including two external layers are designated as symbol 1 and the layers of the second component are designated as symbol 2. The total number of layers, *N*, in such a composite sample is $2n+1$. The number of layers designated as symbol 1 is $n+1$, and the number of layers designated as symbol 2 is n. The layer of each component has some constant thickness and the layers of same component have identical thickness.

According to the design of laminated architecture shown in Fig. 1, the differences in the thermal expansion coefficients of two adjacent components in a laminate structure can lead to a thermal mismatch during cooling from the sintering temperature. This results in a strain mismatch defined as[31]:

$$\varepsilon_M = \int_T^{T_0} (\alpha_2 - \alpha_1) dT \tag{1}$$

Table 1
Weight function coefficients ($A\upsilon\mu$) for a 3-point bend bar determined by the "boundary collocation method".

	$\mu=0$	$\mu=1$	$\mu=2$	$\mu=3$	$\mu=4$
$\upsilon=0$	0.50	2.45	0.07	1.32	−3.07
$\upsilon=1$	0.54	−5.08	24.35	−32.72	18.12
$\upsilon=2$	−0.19	2.56	−12.64	19.76	−10.99

where α_1 and α_2 are the thermal expansion coefficient of the two materials and T_0 is the temperature at which elastic stress develops due to thermal strain mismatch and T is the room temperature. In the ceramic system investigated in the present work where there is perfectly rigid bonding between the layers in a two component system, the residual stresses generated after sintering have been described as[32]:

$$\sigma_{res1} = -\frac{nE_1E_2h_2(\alpha_2-\alpha_1)\ \Delta T}{n(1-\upsilon_1)E_2h_2+(n+1)(1-\upsilon_2)E_1h_1} \tag{2}$$

$$\sigma_{res2} = \frac{(n+1)E_1E_2h_1(\alpha_2-\alpha_1)\ \Delta T}{n(1-\upsilon_1)E_2h_2+(n+1)(1-\upsilon_2)E_1h_1} \tag{3}$$

where E_i and υ_i are the Young's modulus and Poisson's ratio of the *i*th component, respectively, h_1 and h_2 are the layer thickness of the first and second components with thermal expansion coefficients of α_1 and α_2.

Using the superposition principle, the crack-tip stress intensity for an edge crack in a multilayer SENB specimen, $K_{tip}(a)$, can be written as[33]:

$$K_{tip}(a) = K_{appl}(a) + K_{res}(a) \tag{4}$$

where K_{appl} is the stress intensity due to the applied bending load, and K_{res} is the stress intensity due to the designed residual stresses. Then the crack propagation criterion is fulfilled when[33]:

$$K_{appl}(a) \geq K_0 - K_{res}(a) = K_{apparent} \tag{5}$$

where K_0 is the intrinsic toughness of each individual layer calculated by the SENB method in the corresponding monoliths, and $K_{apparent}$ is the apparent fracture toughness of the laminated composites. In Eqs. (4) and (5), the effect of residual stresses on the fracture toughness of the laminated composite, i.e. $K_{res}(a)$, can be evaluated by integrating the product of a weight function $h(x,a)$ and the stress distribution $\sigma_{res}(x)$[34]:

$$K_{res}(a) = \int_0^a h(x,a)\sigma_{res}(x)\ dx \tag{6}$$

The corresponding weight function is given by[35]:

$$h(x,a) = \left(\frac{2}{\pi a}\right)^{1/2} \frac{1}{(1-x/a)^{1/2}(1-a/w)^{3/2}} \times \left[\left(1-\frac{a}{w}\right)^{3/2} + \sum A_{vu}\left(1-\frac{x}{a}\right)^{(v+1)}\left(\frac{a}{w}\right)^{u}\right] \tag{7}$$

where w is the specimen thickness, and the parameters $A\upsilon\mu$, υ and μ determined using the "boundary collocation method"[35] are listed in Table 1.

Table 2
Samples with external compressive layers prepared by hot-pressing.

Samples	Composition		Layer thickness (mm)		N	Layer thickness ratio
	Compressive layers	Tensile layers	Compressive layers	Tensile layers		
LZS-1	ZrB_2 + 30 vol% SiC	ZrB_2 + 10 vol% SiC	0.6	0.6	17	0.89
LZS-2	ZrB_2 + 30 vol% SiC	ZrB_2 + 20 vol% SiC	0.6	0.6	17	0.89
LZS-3	ZrB_2 + 30 vol% SiC	ZrB_2 + 20 vol% SiC	0.4	0.8	17	1.78
LZS-4	ZrB_2 + 30 vol% SiC	ZrB_2 + 20 vol% SiC	0.4	0.5	9	1
LZS-5	ZrB_2 + 30 vol% SiC	ZrB_2 + 20 vol% SiC	0.32	0.6	9	1.5
LZS-6	ZrB_2 + 30 vol% SiC	ZrB_2 + 20 vol% SiC	0.27	0.67	9	2
LZS-7	ZrB_2 + 30 vol% SiC	ZrB_2 + 20 vol% SiC	0.23	0.71	9	2.5
LZS-8	ZrB_2 + 30 vol% SiC	ZrB_2 + 20 vol% SiC	0.2	0.75	9	3
LZS-9	ZrB_2 + 30 vol% SiC	ZrB_2 + 20 vol% SiC	0.13	0.83	9	5

3. Experimental procedure

Commercially available ZrB_2 (mean particle size 2 μm, Northwest Institute for Non-ferrous Metal Research, China) and SiC (mean particle size 0.5 μm, Weifang Kaihua Micro-powder Co. Ltd., China) were used in the present work. The processing procedure of the laminated ZrB_2–SiC ceramics included: (a) ball milling of powders in certain proportions, and (b) stacking layers in alternated sequence in graphite mold. The mixtures of various compositions were ball-milled using ZrO_2 ball and ethanol as the grinding media at 220 rpm for 10 h, followed by rotating evaporation to remove the solvent. The obtained powders were put into graphite die according to a certain quality ratio. Both monolithic and laminated samples were fabricated. The laminated samples were prepared by alternately stacking compressive layers and tensile layers with different SiC contents. The monolithic samples were fabricated from stacking layers with the same composition. The hot pressing was performed at 1950 °C and 30 MPa for 60 min in Ar atmosphere. The specimens for mechanical tests were obtained by machining the hot pressed tiles. All flexural and fracture bars were cut with the tensile surface perpendicular to the hot-pressing direction. A minimum number of six specimens were tested for each experimental condition. The macroscopic cross-section and microstructures features of the composites were observed by optical microscope and scanning electron microscopy, respectively. Both the intrinsic fracture toughness K_0 of the monolithic sample and the apparent fracture toughness (K_{IC}) of the laminated sample were evaluated by a single-edge notched beam (SENB) test with a 16-mm span in three point bending and a cross-head speed of 0.05 mm/min using 2 mm × 4 mm × 22 mm bars. The elastic modulus was measured by three-points bending tests with a 30-mm span by using a calibrated strain gauge to measure the strain as a function of applied load and a cross-head speed of 0.5 mm/min using 3 mm × 4 mm × 36 mm bars.

4. Results and discussion

In the present work, the laminated ZrB_2–SiC ceramics were designed according to Fig. 1 and the characteristics of samples with external compressive layers prepared by hot-pressing are listed in Table 2. The optical micrographs of cross-section of the laminated ZrB_2–SiC ceramics with different compositions and layer thickness are shown in Fig. 2. It can be seen that layers in the laminated ceramics are smooth and uniform. The perfect adhesion between layers is evident. It should be noted that the residual thermal stress adjustment is very important and too high residual tensile stress will cause the material to crack (Fig. 2a).

4.1. Thermal expansion coefficient adjustment

In order to introduce residual stresses in laminated structures, it is necessary to use materials with different coefficients of thermal expansion as discussed in Section 2. In this work, the differences in the thermal expansion coefficient are gained through adjusting the SiC content in the single lamina. According to Eqs. (2) and (3), for the given geometry parameters of laminated architecture, the thermal expansion coefficient directly decides the residual stresses and affects the microstructure and mechanical reliability. Fig. 2 shows the effect of thermal expansion coefficient mismatch on the laminated ZrB_2–SiC ceramics. In Fig. 2a, many cracks emerge and propagate through the tensile layers in LZS-1. But there are no cracks in LZS-2–LZS-9. The two phenomena suggest that the thermal expansion coefficient adjustment is very effective and important. A higher difference in the thermal expansion coefficient was expected in order to obtain a bigger residual compressive stress. Meanwhile, it must be ensured that the residual tensile stresses are less than the strength of tensile layers.

4.2. Residual stress in the laminated ZrB_2–SiC ceramics

The residual stress profile developed within a ceramic laminate is related to the composition/microstructure, thickness and stacking order of the monolayer, i.e. the composite architecture. On the basis of the aforementioned analysis, as long as the Young modulus, Poisson's ratio, thermal expansion coefficient and thickness for each layer are determined, the residual stress distribution will can be estimated for the preset laminated architecture. For the designed laminated architecture as shown in Fig. 1, we can define a variable, $\lambda = nh_2/(n+1)h_1$, which is the ratio between the total thickness of the tensile layers and that of

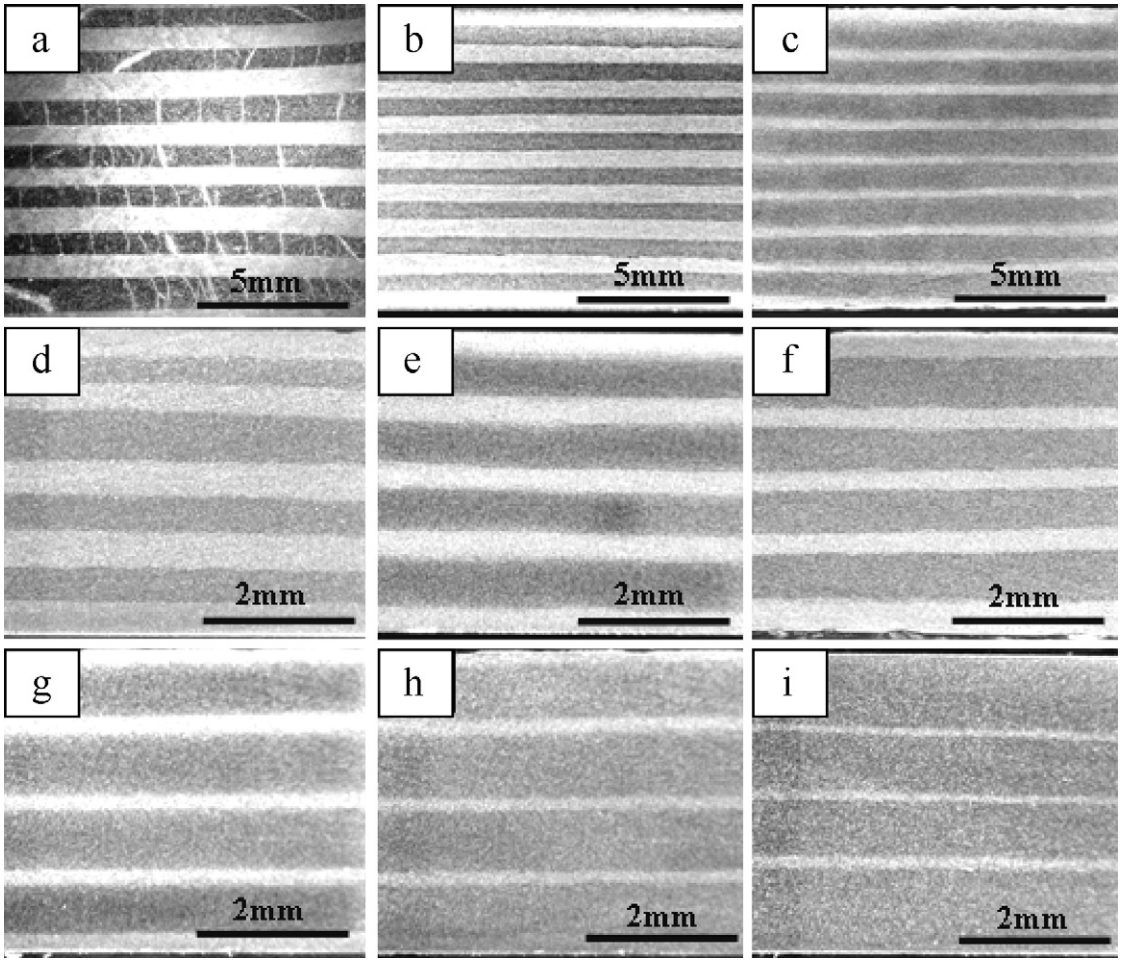

Fig. 2. Optical micrographs of cross-section of the laminated ZrB_2–SiC ceramics: (a)–(i) represent LZS-1–LZS-9, respectively.

the compressive layers. Thus Eqs. (2) and (3) can be simplified as:

$$\sigma_{res1} = -\frac{E_1 E_2(\alpha_2 - \alpha_1)\ \Delta T}{(1-\upsilon_1)E_2 + (1-\upsilon_2)E_1\lambda^{-1}} \quad (8)$$

$$\sigma_{res2} = \frac{E_1 E_2(\alpha_2 - \alpha_1)\ \Delta T}{(1-\upsilon_1)E_2\lambda + (1-\upsilon_2)E_1} \quad (9)$$

As it derives from Eqs. (8) and (9), the architecture (λ) defines the residual stress field. We have estimated the residual stresses of LZS-4–LZS-9 according to Eqs. (8) and (9). The properties of the materials required for the residual stress calculation are summarized in Table 3. The Poisson's ratio was calculated using rule of mixture taking literature values for the Poisson's ratio of the two constituent phases ($ZrB_2 = 0.121$, SiC = 0.17).[36] The thermal expansion coefficient values for ZrB_2 + 20 vol% SiC and ZrB_2 + 30 vol% SiC were 7.18×10^{-6}/K[37] and 6.8×10^{-6}/K. [38]

Fig. 3 shows the residual stresses for different layer thickness ratios (λ) in the layered architectures designed with external compressive layers. As shown in Fig. 3, the compressive stress increases with increasing layer thickness ratio, whereas the tensile stress decreases. For the laminated ceramics, the residual compressive stress is beneficial to the mechanical properties and mechanical reliability.[24,28] Therefore, a high λ should be applied in order to achieve high residual compressive stress during the design of laminate ceram-

Table 3
Material properties used to estimate the residual stress distribution.

Monolithic material	E (GPa)	Poisson's ratio, ν	Thermal expansion coefficient, α (10^{-6}/K)	K_0 (MPam$^{1/2}$)
ZrB_2 + 20 vol% SiC	450	0.131	7.18[a]	4.8
ZrB_2 + 30 vol% SiC	440	0.136	6.8[b]	5.6

[a] Ref. [37].
[b] Ref. [38].

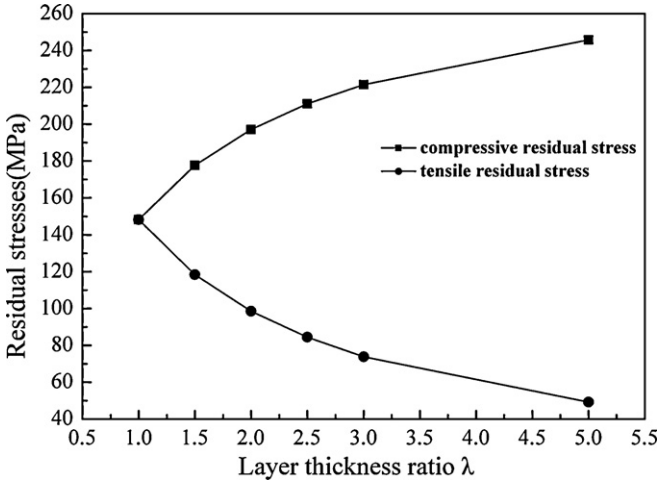

Fig. 3. Magnitude of the residual stresses which develop in the layers for several geometries as a function of the layer thickness ratio (λ).

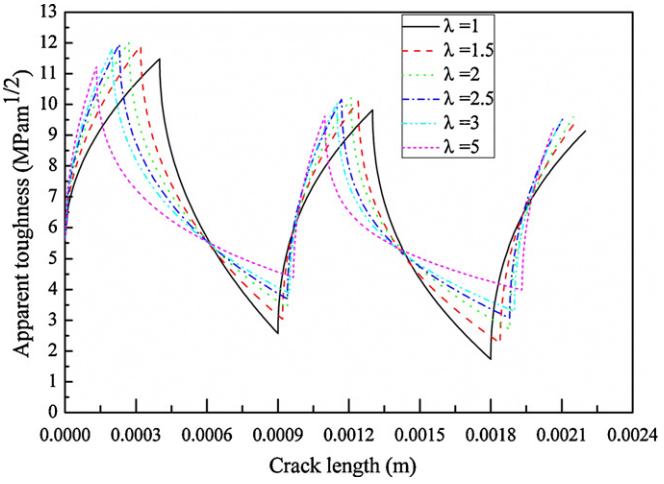

Fig. 4. Apparent toughness as a function of the layer thickness ratio (λ) in the layered architectures designed with external compressive layers.

ics. However, the highest residual compressive stress (the highest λ) does not correspond to the highest apparent toughness according to the theoretical calculations as shown in Fig. 4.

4.3. Apparent fracture toughness of the laminated ZrB_2–SiC ceramics

The apparent fracture toughness has been evaluated according to Eqs. (5)–(7). Undoubtedly, toughening in laminated

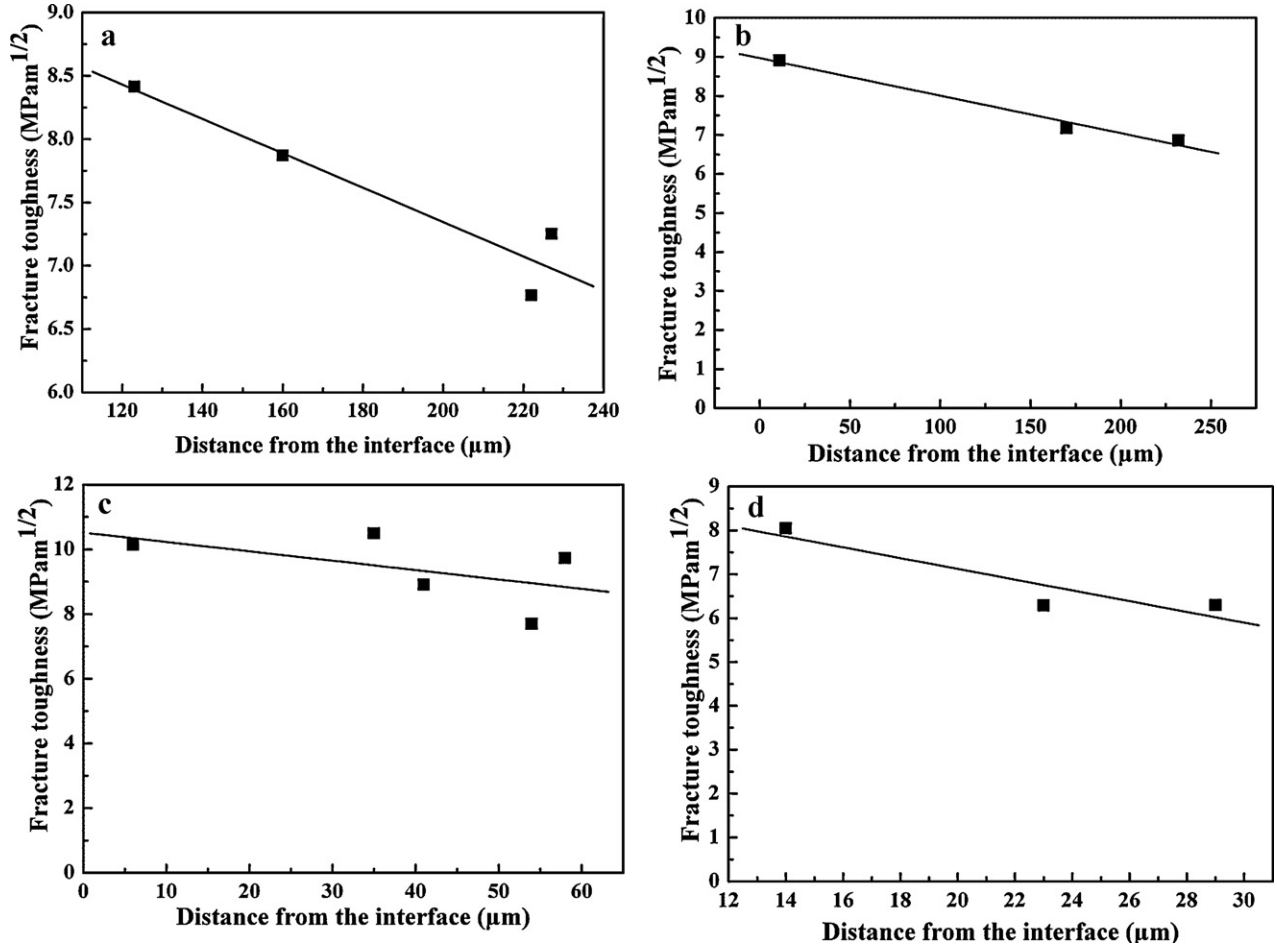

Fig. 5. The experimental values of fracture toughness as a function of the distance between the notched tip and the nearest ZrB_2 + 30 vol% SiC/ZrB_2 + 20 vol% SiC interface: (a) λ = 1, (b) λ = 2, (c) λ = 3 and (d) λ = 5 represent different layer thickness ratios, respectively.

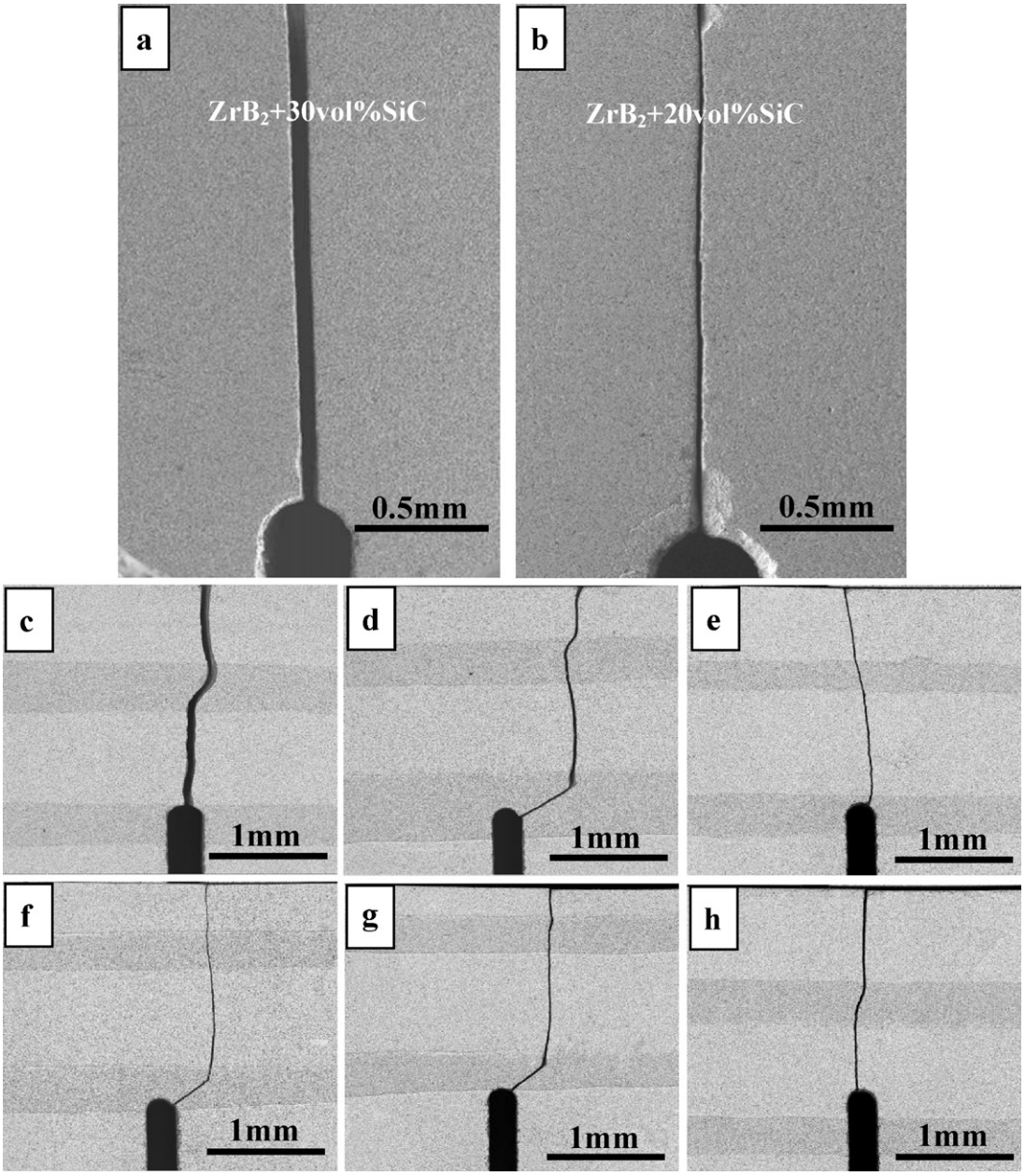

Fig. 6. SEM images of cross-section of the monolithic (a and b) and laminated (c–h) ceramics specimens after SENB test.

ceramics occurs as a result of the residual compressive stresses shielding the applied stress at the crack tip.[29] Fig. 4 shows the apparent fracture toughness as a function of crack length for different layer thickness ratios (λ) in the layered architectures, i.e. laminated LZS-4–LZS-9 designed with external compressive layers. As it can be inferred from Eqs. (8) and (9), the residual stress field is influenced by the architectural parameter λ. Therefore, the apparent fracture toughness is represented for different values of λ (until the crack length a being approximately half of the specimen thickness) in order to determine the geometry that provides the maximum shielding. It can be found from Fig. 4 that the laminated ZrB_2–SiC architecture maximizes the apparent toughness at the first interface. The toughness increases in the compressive layers with increasing crack length and reaches a local maximum at the ZrB_2 + 30 vol% SiC/ZrB_2 + 20 vol% SiC interface, whereas it decreases in the tensile layers and reaches a local minimum at the ZrB_2 + 20 vol% SiC/ZrB_2 + 30 vol% SiC interface.

In view of the shielding effects as a function of the various λ, the following aspects may be inferred from Fig. 4. For the laminates with residual surface compression, the λ is defined as $nh_2/(n+1)h_1$. Thus, high values of λ correspond to thin ZrB_2 + 30 vol% SiC layers in comparison to the ZrB_2 + 20 vol% SiC layers, and high compressive stresses are present in the former according to Eq. (8). This is the reason why the shielding increases sharply in the ZrB_2 + 30 vol% SiC layers and a high

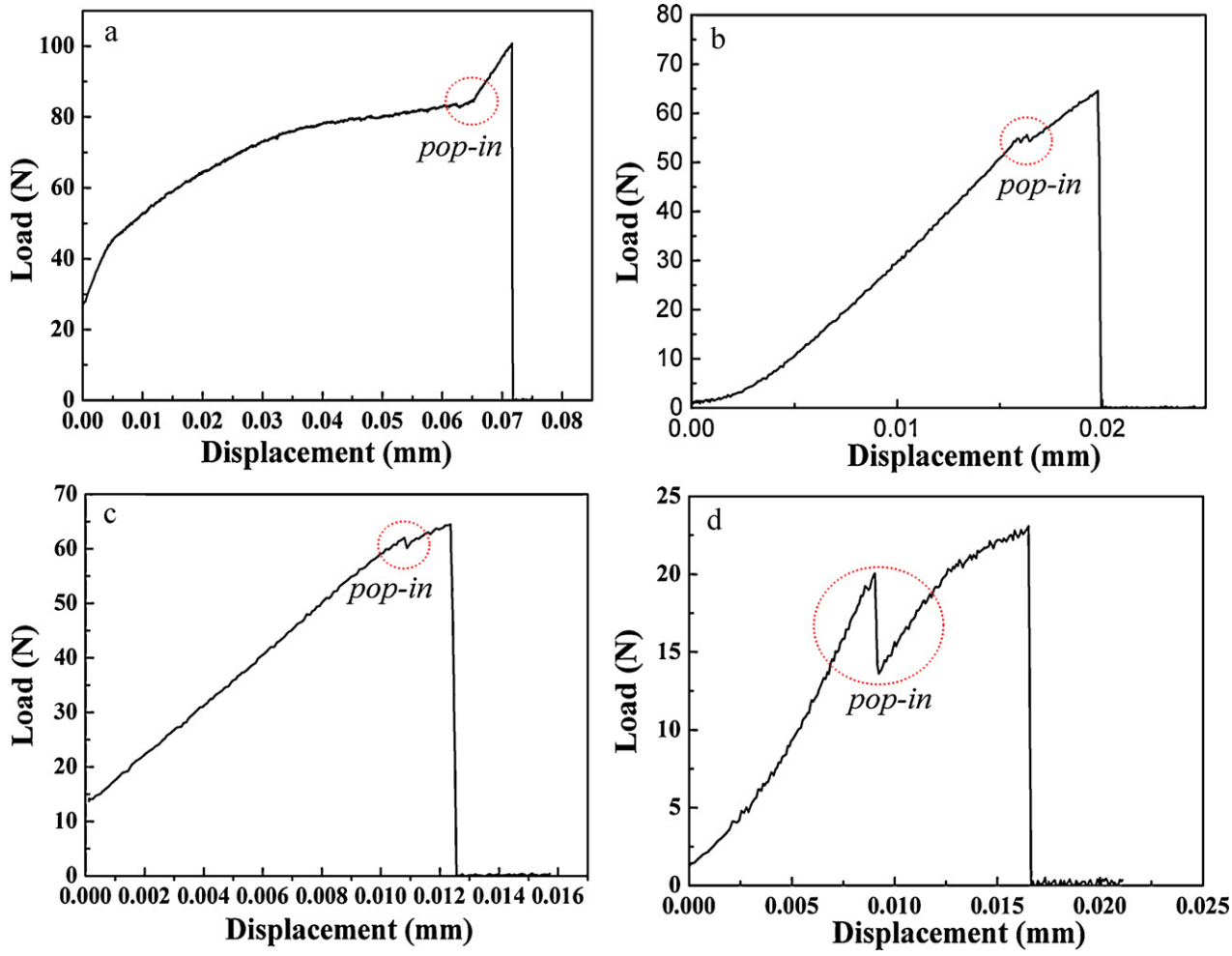

Fig. 7. The effect of the location of crack tips on the load–displacement curve of laminated ceramic: (a), (b), (c), and (d) laminated ceramic specimens c, d, g, and h, respectively.

stress intensity factor should be considered to lead the specimen to failure.[33] However, for low values of λ, the thickness of the ZrB_2 + 30 vol% SiC layers is much greater than that of the ZrB_2 + 20 vol% SiC layers. As a result, high tensile stresses arise in these ZrB_2 + 20 vol% SiC layers and the effective toughness drops remarkably in the ZrB_2 + 20 vol% SiC layers for these laminates. In contrast to what could be expected, the highest surface compressive stress (the highest λ) does not correspond to the highest shielding in the first layer. Since the maximum shielding in the first layer is obtained at a distance equal to the outer layer thickness, the thickness h_1 plays an important role.

The values of fracture toughness obtained by SENB tests for LZS-4, 6, 8 and 9 are shown in Fig. 5. It should be noted that the notch tips were located in the fifth layer of the tested samples. As shown in Fig. 5, the experimental value of the fracture toughness is a function of the distance from notch tip to the ZrB_2 + 30 vol% SiC/ZrB_2 + 20 vol% SiC interface. Note that the interface is the nearest ZrB_2 + 30 vol% SiC/ZrB_2 + 20 vol% SiC interface along the direction of crack advancing. The fracture toughness can reach the maximum at the ZrB_2 + 30 vol% SiC/ZrB_2 + 20 vol% SiC interface, which is consistent with the theoretical calculations as shown in Fig. 4. In addition, the fracture toughness increases with the increase of layer thickness ratio (λ) when λ is lower value, and then decreases as the layer thickness ratio (λ) continues to increase. It also agrees with the theoretical calculations that the highest λ does not correspond to the highest fracture toughness. The maximum of fracture toughness is 10.4 $MPam^{1/2}$ when λ is 3.

4.4. Crack propagation in the laminated ceramics and toughening mechanism

The crack growth resistance was obviously affected by the presence of residual stresses in the laminated ZrB_2–SiC ceramics due to the differential thermal strains between adjacent layers during cooling down from sintering. So, crack propagation in the laminated ceramics will be swayed by the residual stresses. SEM images of cross-section of the monolithic and laminated ceramics specimens after SENB tests are shown in Fig. 6. These laminated ceramic specimens used for crack propagation analysis come from LZS-9 listed in Table 2. As shown in Fig. 6c–h, the ZrB_2 + 30 vol% SiC layers show dark and thin, while the ZrB_2 + 20 vol% SiC layers appear as bright and thick layers separating the ZrB_2 + 30 vol% SiC layers. It can be observed that cracks are deflected in laminated ceramics and no crack deflection is observed in the monolithic samples. In addition,

the modes of crack propagation are dependent on the location of crack tips. When crack tips were located in the compressive layers (see Fig. 6d–g), the initial crack deflection would occur at the tips. But cracks perforate through the tensile layers when crack tips located in the tensile layers (see Fig. 6h) or at the compressive layer/tensile layer interfaces (see Fig. 6c). Furthermore, when crack tips were located in the tensile layers or compressive layer/tensile layer interfaces (see Fig. 6c and h), cracks deflection would occur as long as the cracks propagate into the next compressive layer. The change of crack propagation direction implies that the residual compressive stresses can weaken the crack propagation driving force and enhance the crack growth resistance. This is why the laminated ceramics with strong interfaces exhibit high fracture toughness. Another feature of laminated composites worthy of note is their fracture behavior under flexural loading. The representative load–displacement curves of the notched laminated ceramic specimens (laminated ceramic specimens c, d, g, h related to Fig. 6) are shown in Fig. 7. As can be seen, the laminated ceramic shows a stepwise fracture with a pop-in event in the load–displacement curve. This behavior has been observed by other authors in other laminated structures, exhibiting the effectiveness of the internal compressive layers in hindering the cracks propagation.[26,29] As it can be inferred from Fig. 7, the pop-in events accompany crack deflection referred to results as shown in Fig. 6. After pop-in events the unstable failure does not emerge. Instead, the fracture stress increases continuously with a different slope because the crack propagation is inhibited by the residual compressive stresses. The significant differences in crack propagation and fracture behavior between the laminated and monolithic ZrB_2–SiC ceramics reflect the toughening effect of the residual stresses.

5. Conclusions

The laminated ZrB_2–SiC ceramics were successfully prepared by hot-pressing through superimposing different ceramic layers. The maximum apparent fracture toughness of these laminated ZrB_2–SiC ceramics was 10.4 $MPam^{1/2}$, which was much higher than that of monolithic ZrB_2–SiC ceramics. The theoretical calculations indicated that the residual stresses and apparent toughness were strongly dependent on the architectural parameter and the highest residual compressive stress did not correspond to the highest apparent toughness. The results of SENB tests showed that the experimental values of the fracture toughness of laminated ZrB_2–SiC ceramics were defined by the position of the notch tips inside compressive or tensile layers, which was in agreement with the results predicted by the weight function analytical procedure. In addition, both the fracture behavior and the patterns of crack propagation of the laminated ceramics were dependent on the position of crack tips which were located in the compressive or tensile layers. The crack deflection and pop-in events in the load–displace curve occurred because of the residual compressive stresses enhancing the crack growth resistance.

Acknowledgements

This work was supported by the National Science Foundation (51072042) of China, project (HIT.KLOF.2009026) supported by the Key laboratory Opening Funding of National Key Laboratory on Advanced Composites in Special Environment and the National Science Foundation for Post-doctoral Scientists of China.

References

1. Fahrenholtz WG, Hilmas GE, Talmy IG, Zaykoski JA. Refractory diborides of zirconium and hafnium. *J Am Ceram Soc* 2007;**90**(5):1347–64.
2. Opeka MM, Talmy IG, Wuchina EJ, Zaykoski JA, Causey SJ. Mechanical, thermal, and oxidation properties of refractory hafnium and zirconium compounds. *J Eur Ceram Soc* 1999;**19**:2405–14.
3. Wang Z, Hong CQ, Zhang XH, Sun X, Han JC. Microstructure and thermal shock behavior of ZrB_2–SiC-graphite composite. *Mater Chem Phys* 2009;**113**:338–41.
4. Zhang XH, Xu L, Han WB, Weng L, Han JC, Du SY. Microstructure and properties of silicon carbide whisker reinforced zirconium diboride ultra-high temperature ceramics. *Solid State Sci* 2009;**11**:156–61.
5. Wang Z, Wang S, Zhang XH, Hu P, Han WB, Hong CQ. Effect of graphite flake on microstructure as well as mechanical properties and thermal shock resistance of ZrB_2–SiC matrix ultrahigh temperature ceramics. *J Alloys Compd* 2009;**484**:390–4.
6. Li WJ, Zhang XH, Hong CQ, Han WB, Han JC. Preparation, microstructure and mechanical properties of ZrB_2–ZrO_2 ceramics. *J Eur Ceram Soc* 2009;**29**:779–86.
7. Liu Q, Han WB, Zhang XH, Wang S, Han JC. Microstructure and mechanical properties of ZrB_2–SiC composites. *Mater Lett* 2009;**63**:1323–5.
8. Yang FY, Zhang XH, Han JC, Du SY. Mechanical properties of short carbon fiber reinforced ZrB_2–SiC ceramic matrix composites. *Mater Lett* 2008;**62**:2925–7.
9. Zhang P, Hu P, Zhang XH, Han JC, Meng SH. Processing and characterization of ZrB_2–SiC_W ultra-high temperature ceramics. *J Alloys Compd* 2009;**472**:358–62.
10. Zhang XH, Xu L, Du SY, Liu CY, Han JC, Han WB. Spark plasma sintering and hot pressing of ZrB_2–SiC_W ultra-high temperature ceramics. *J Alloys Compd* 2008;**466**:241–5.
11. Zhao Y, Wang LJ, Zhang GJ, Jiang W, Chen LD. Preparation and microstructure of a ZrB_2–SiC composite fabricated by the spark plasma sintering-reactive synthesis (SPS-RS) method. *J Am Ceram Soc* 2007;**90**(12):4040–2.
12. Zhang SC, Hilmas GE, Fahrenholtz WG. Pressureless densification of zirconium diboride with boron carbide additions. *J Am Ceram Soc* 2006;**89**:1544–50.
13. Sciti D, Guicciardi S, Bellosi A, Pezzotti G. Properties of a pressureless-sintered ZrB_2–$MoSi_2$ ceramic composite. *J Am Ceram Soc* 2006;**89**:2320–2.
14. Zhang XH, Li WJ, Hong CQ, Han WB, Han JC. Microstructure and mechanical properties of hot pressed ZrB_2–SiC_p–ZrO_2 composites. *Mater Lett* 2008;**62**:2404–6.
15. Zhang XH, Wang Z, Sun X, Han WB, Hong CQ. Effect of graphite flake on the mechanical properties of hot pressed ZrB_2–SiC ceramics. *Mater Lett* 2008;**62**:4360–2.
16. Jiménez-Melendo M, Clauss C, DomÍnguez-RodrÍguez A, Sánchez-Herencia AJ, Moya JS. Microstructure and high-temperature mechanical behavior of alumina/alumina–yttria-stabilized tetragonal zirconia multilayer composites. *J Am Ceram Soc* 1997;**80**(8):2126–30.
17. Sciti D, Nagliati M, Tochino S, Pezzotti G, Guicciardi S. Fabrication and residual stresses characterization of novel non-oxide multilayer ceramics. *J Eur Ceram Soc* 2006;**26**:3415–23.
18. Lakshminarayanan R, Shetty DK, Cutler RA. Toughing of layered ceramic composites with residual surface compression. *J Am Ceram Soc* 1996;**79**(1):79–87.

19. Portu G, Micele L, Pezzotti G. Laminated ceramic structures from oxide systems. *Composites: Part B* 2006;**37**:556–67.
20. Bueno S, BaudÍn C. Layered materials with high strength and flaw tolerance based on alumina and aluminium titanate. *J Eur Cer Soc* 2007;**27**:1455–62.
21. Mawdsley JR, Kovar D, Halloran JW. Fracture behaviour of alumina/monazite multilayer laminates. *J Am Ceram Soc* 2000;**83**(4):802–8.
22. Wang CA, Huang Y, Zan QF, Guo H, Cai SY. Biomimetic structure design—a possible approach to change the brittleness of ceramics in nature. *Mater Sci Eng C* 2000;**11**:9–12.
23. Clegg WJ, Kendall K, Alford NM, Button TW, Birchall JD. A simple way to make tough ceramics. *Nature* 1990;**347**:455–7.
24. Lugovy M, Slyunyayev V, Subbotin V, Orlovskaya N, Gogotsi G. Crack arrest in Si_3N_4-based layered composites with residual stress. *Comp Sci Technol* 2004;**64**:1947–57.
25. Sglavo VM, Bertoldi M. Design and production of ceramic laminates with high mechanical resistance and reliability. *Acta Mater* 2006;**544**:929–37.
26. Bermejo R, Torres Y, Sanchez-Herencia AJ, Baudín C, Anglada M, Llanes L. Residual stresses, strength and toughness of laminates with different layer thickness ratios. *Acta Mater* 2006;**54**:4745–57.
27. Pavese M, Fino P, Ortona A, Badini C. Potential of SiC multilayer ceramics for high temperature applications in oxidising environment. *Ceram Int* 2008;**34**:197–203.
28. Sglavo VM, Paternoster M, Bertoldi M. Tailored residual stresses in high reliability alumina–mullite ceramic laminates. *J Am Ceram Soc* 2005;**88**(10):2826–32.
29. Lugovy M, Slyunyayev V, Orlovskaya N, Blugan G, Kuebler J, Lewis M.vadjust
Apparent fracture toughness of Si_3N_4-based laminates with residual compressive or tensile stresses in surface layers. *Acta Mater* 2005;**53**: 289–96.
30. Rao MP, Sánchez-Herencia AJ, Beltz GE, McMeeking RM, Lange FF. Laminar ceramics that exhibit a threshold strength. *Science* 1999;**286**:102–5.
31. Ho S, Hillman C, Lange FF, Suo Z. Surface cracking in layers under biaxial residual compressive stress. *J Am Ceram Soc* 1995;**78**(9): 2353–7.
32. Chartier T, Mlerle D, Besson JL. Laminar ceramic composites. *J Eur Ceram Soc* 1995;**15**:101–7.
33. Bermejo R, Pascual J, Lube T, Danzer R. Optimal strength and toughness of Al_2O_3–ZrO_2 laminates designed with external or internal compressive layers. *J Eur Ceram Soc* 2008;**28**:1575–83.
34. Bueckner HF. A novel principle for the computation of stress intensity factors. *Z Angew Math Mech* 1970;**50**(9):529–46.
35. Fett T, Munz D. Influence of crack–surface interactions on stress intensity factor in ceramics. *J Mater Sci Lett* 1990;**9**:1403–6.
36. Grigoriev ON, Galanov BA, Kotenko VA, Ivanov SM, Koroteev AV, Brodnikovsky NP. Mechanical properties of ZrB_2–SiC ($ZrSi_2$) ceramics. *J Eur Ceram Soc* 2010;**30**:2173–81.
37. Loehman R, Corral E, Dumm HP, Kotula P, Tandon R. Ultra high temperature ceramics for hypersonic vehicle applications. Sandia report; 2006. Sand 2006-2925.
38. Zimmermann JW, Hilmas GE, Fahrenholtz WG. Thermophysical properties of ZrB_2 and ZrB_2–SiC ceramics. *J Am Ceram Soc* 2008;**91**(5): 1405–11.